Effects of grain size and seawater salinity on magnesium hydroxide dissolution and secondary calcium carbonate precipitation kinetics: implications for ocean alkalinity enhancement

Charly A. Moras[1*], Tyler Cyronak[2], Lennart T. Bach[3], Renaud Joannes-Boyau[1] and Kai G. Schulz[1]

[1]Faculty of Science and Engineering, Southern Cross University, Lismore, NSW, Australia
[2]Institute for Coastal Plain Science, Georgia Southern University, Savannah, GA, USA
[3]Ecology & Biodiversity, Institute for Marine and Antarctic Studies, University of Tasmania, Hobart, TAS, Australia

Correspondence: Charly A. Moras (c.moras.10@student.scu.edu.au)

Abstract. Understanding the impact that mineral grain size and seawater salinity have on magnesium hydroxide ($Mg(OH)_2$) dissolution and secondary calcium carbonate ($CaCO_3$) precipitation is critical for the success of ocean alkalinity enhancement. We tested the $Mg(OH)_2$ dissolution kinetics in seawater using three $Mg(OH)_2$ grain sizes (<63, 63-180 and >180 µm) and at three salinities (~36, ~28 and ~20). While $Mg(OH)_2$ dissolution occurred quicker the smaller the grain size, salinity did not significantly impact measured rates. Our results also demonstrate that grain size can impact secondary $CaCO_3$ precipitation, suggesting that an optimum grain size exists for ocean alkalinity enhancement (OAE) using solid $Mg(OH)_2$. Of the three grain sizes tested, the medium grain size (63-180 µm) was optimal in terms of delaying secondary $CaCO_3$ precipitation. We hypothesize that in the lowest grain size experiments, the higher surface area provided numerous $CaCO_3$ precipitation nuclei, while the slower dissolution of bigger grain size maintained a higher alkalinity and pH at the surface of particles, increasing $CaCO_3$ precipitation rates and making it observable much quicker than for the intermediate grain size. Salinity also played a role in $CaCO_3$ precipitation where the decrease in magnesium (Mg) allowed for secondary precipitation to occur more quickly, similar in effect size to another known inhibitor, i.e., dissolved organic carbon (DOC). In summary, our results suggest that OAE efficiency as influenced by $CaCO_3$ precipitation not only depends on seawater composition but also on the physical properties of the alkaline feedstock used.

1. Introduction

The concentration of carbon dioxide (CO_2) in the atmosphere has been in a relatively narrow band from ~180 to ~280 ppmv for the last 800,000 years, but has risen rapidly over the last 250 years to approximately 420 ppmv today (Lüthi et al., 2008, Monnin et al., 2001, Siegenthaler et al., 2005). This is the result of increasing utilisation of fossil fuels, cement production and land-use change, driving subsequent global climate change (IPCC, 2021). While about 42% of CO_2 emissions remain in the atmosphere, and are mainly responsible for global warming, about 26% are currently absorbed by the oceans, leading to ocean acidification (Friedlingstein et al., 2022, IPCC, 2021). To locally mitigate the effects of ocean acidification and slow down the increase in Earth's global temperature, CO_2 reduction efforts are not sufficient and the use of carbon dioxide removal (CDR) strategies have become necessary as a supplement to emission reduction (Hoegh-Guldberg et al., 2019).

One emerging marine CDR approach is ocean alkalinity enhancement (OAE). Over long timescales, the natural CO_2-facilitated weathering of alkaline rocks supplies alkalinity to the oceans, influencing its CO_2 uptake potential and storage. OAE builds upon this weathering feedback in the Earth System and can be accomplished by actively spreading pulverized alkaline minerals in and around marine environments or electrochemically removing acidity from seawater (Eisaman et al., 2023). In both cases, the seawater total alkalinity (TA) is increased thereby increasing the storage capacity of seawater for atmospheric CO_2 (GESAMP, 2019, Kheshgi, 1995). On local scales around where the OAE perturbation is made, the increase in alkalinity and pH may also mitigate ocean acidification (Hartmann et al., 2013).

Recent studies have investigated the carbonate chemistry changes following OAE, and a major outcome was the risk for runaway calcium carbonate ($CaCO_3$) precipitation (Fuhr et al., 2022, Hartmann et al., 2023, Moras et al., 2022). There are several inorganic $CaCO_3$ precipitation mechanisms that have been described in the literature (Morse et al., 2007, Pytkowicz, 1965). $CaCO_3$ can precipitate homogeneously in the absence of solid or soluble organic and inorganic particles, pseudo-homogeneously in the presence of organic surfaces, and heterogeneously in the presence of mineral solids (Marion et al., 2009). The key parameter that governs whether precipitation occurs is the calcium carbonate saturation state (Ω), which is calculated from seawater Ca^{2+} and CO_3^{2-} concentrations as:

$$\Omega = \frac{[Ca^{2+}]\,[CO_3^{2-}]}{K_{sp}}$$

where $[Ca^{2+}]$ and $[CO_3^{2-}]$ are the concentrations of calcium and carbonate in solution, respectively, and K_{sp} the solubility product of $CaCO_3$ in the solution. Ω is therefore closely related to the composition of the solution and its salinity, but is also highly temperature dependent (Zeebe and Wolf-Gladrow, 2001). For aragonite, the $CaCO_3$ morphotype that inorganically

precipitates in modern seawater, the saturation state (Ω_A) has to be higher than 12.3 for pseudo-homogeneous precipitation to occur in water with a salinity of 35 and at 25 ºC (Marion et al., 2009). Homogeneous precipitation will occur at much higher Ω_A values, while heterogeneous precipitation will occur already at much lower Ω_A but depends on the actual lattice compatibility of $CaCO_3$ for the mineral particles present (Morse et al., 2007, Zhong and Mucci, 1989). Another important aspect is that once precipitation becomes measurable, it will continue in a "runaway" fashion, i.e., quickly ramping up until it slows down once Ω_A gets closer to 1 again.

Several studies have reported such behaviour upon mineral alkalinity addition (Fuhr et al., 2022, Hartmann et al., 2023, Moras et al., 2022) with critical threshold of Ω_A of ~7.0 for the two calcium based OAE minerals of calcium oxide – CaO – and calcium hydroxide – $Ca(OH)_2$ – and report precipitation stopping at Ω_A values of 1.8-2.0 (Moras et al., 2022). Precipitation has also been observed for magnesium-based minerals such as brucite or reagent grade magnesium hydroxide – $Mg(OH)_2$, but actual thresholds have not been determined (Hartmann et al., 2023). Furthermore, the effect of grain size, determining factor of the surface area available for mineral dissolution and $CaCO_3$ precipitation, has not been studied. Similarly, the effect of potential $CaCO_3$ precipitation inhibitors such as seawater magnesium (Mg) concentrations, governed by salinity, and dissolved organic carbon (DOC), are relatively unknown (Chave and Suess, 1970, Millero et al., 2001, Pan et al., 2021, Zhong and Mucci, 1989). This study focuses on the impact of $Mg(OH)_2$ grain size on its dissolution kinetics in natural seawater, as well as the impact of salinity. Furthermore, the subsequent runaway $CaCO_3$ precipitation that is triggered, and its kinetics are reported. Finally, the effect of increased [Mg] and [DOC] in seawater on the $CaCO_3$ precipitation process is explored.

2. Material and methods

2.1. Seawater collection and experimental setup

Seawater was collected in Broken Head, New South Wales, Australia (25°42'12'' S, 153°37'03'' E) using 25 L jerry cans, about 200 m from the shore to avoid sampling sand and suspended particles. The collected seawater was stored in the dark at 4 °C for three days to reduce microbial activity and allow particles to settle to the bottom, facilitating filtration. The entire contents of the jerry cans were then sterile filtered using a peristaltic pump and a 0.2 µm Whatman Polycap 75 AS filter, before being stored in cleaned and autoclaved 25 L polycarbonate bottles. Prior to conducting the experiments, each seawater batch was equilibrated to laboratory air pCO_2 by bubbling them with H_2O-saturated air for at least a week (Moras et al., 2023). This ensured comparable starting conditions for the various experiments, with a calculated starting pCO_2 of 420.6 ±28.6 µatm in all experiments. All experiments utilised reagent grade $Mg(OH)_2$ (>98%, kindly supplied by Atlas Materials) which had been ground in a Pulverizer laboratory mill.

2.2. Grain size and salinity experiments

Approximately 1.5 litres of seawater were placed in a clean 2 L borosilicate 3.3 beaker, surrounded by a water jacket set to 21 °C and controlled by a tank chiller line TK-1000. A floating lid with three ports was placed on the water surface, allowing for concurrent $Mg(OH)_2$ addition, pH measurement and water sampling. Upon $Mg(OH)_2$ addition, the seawater was incubated for 18 hours to allow for full $Mg(OH)_2$ dissolution. Thereafter the beaker content was transferred to a clean 1 L borosilicate 3.3 Schott bottle which was tightly closed without any headspace to minimise CO_2 ingassing. The bottle was placed on a stirring platform at 200 rpm in the dark, at room temperature (24.8 ±1.3 °C). All grain size and salinity treatments were run in triplicates for up to 34 days.

For the grain size experiments, three grain size ranges were produced using two stainless steel sieves with 63 µm and 180 µm mesh sizes. The medium range, i.e., 63-180 µm, was also used for the salinity experiments at ~36, ~28 and ~20. The lower salinity seawater was produced by mixing natural seawater with MilliQ water. Exact salinities were determined on 200 mL of seawater sample equilibrated to room temperature in a gas tight polycarbonate container, by measuring conductivity and temperature with a 914 pH/conductometer, and converted to salinity using the 1978 practical salinity scale (Lewis and Perkin, 1981). For all experiments, $Mg(OH)_2$ additions were adjusted to yield an Ω_A of ~9 (Table 1) to allow for a significant TA increase and secondary $CaCO_3$ precipitation, based on previously found thresholds for CaO and $Ca(OH)_2$, and with the assumption that the $CaCO_3$ inhibition role of Mg^{2+} requires a higher Ω_A for $CaCO_3$ precipitation within days (Moras et al., 2022). Varying amount of $Mg(OH)_2$ were used in the salinity experiments. The decrease in dissolved [Ca] following dilution with MilliQ led to higher amounts of $Mg(OH)_2$ to be added with decreasing salinity to reach a similar Ω_A of about 9. Furthermore, preliminary tests conducted with the $Mg(OH)_2$ powder used for these experiments, despite having reagent grade properties (>98% pure), have shown that only about 75% of the theoretical maximum TA was generated. Therefore, the $Mg(OH)_2$ additions were adjusted accordingly, with additions varying from 23.3 mg kg^{-1} in the salinity 36 experiments (and all grain size experiments) to 30.2 mg kg^{-1} in the salinity 20 experiments.

In all the experiments, the first 18 hours of reaction were monitored by measuring the pH on the free scale (pH_F) with an Aquatrode Plus with Pt1000 (Metrohm) connected to an 888 Titrando (Metrohm), before transferring the content of the 2 L beaker into the clean 1 L Schott bottles. A sample for TA and DIC measurements was taken before $Mg(OH)_2$ addition, and after the 18 hours. The temperature and pH_F were then recorded twice a day until a sudden drop in pH_F was observed, linked to $CaCO_3$ precipitation. A new sample for TA and DIC measurements was then taken. The time at which $CaCO_3$ runaway precipitation was deemed to have started was considered to be the last stable pH_F measurement before the sudden drop. TA and DIC samples were taken at varying intervals during $CaCO_3$ precipitation (see figures 2 and 4) to cover most of the $CaCO_3$ precipitation process, and at least 300 mL of water was reserved for two TA and DIC samples at the end of the experiment.

Between 9 and 10 TA and DIC samples per experiment were collected to monitor the changes in DIC and TA overtime. Their decrease in a 2:1 ratio was further used to reconstruct TA and DIC from pH measurements in the experiments on the effect of Mg and DOC on $CaCO_3$ precipitation (see below for details).

Table 1: Summary of the main experimental parameters for each of the incubations investigating the salinity and grain size effects on $Mg(OH)_2$ dissolution and $CaCO_3$ precipitation kinetics. "Days of stable TA" encompasses the time between maximum ΔTA recorded and the start of $CaCO_3$ runaway precipitation.

Experimental details	Starting Conditions		Conditions after Full Dissolution			End Conditions		
	Starting TA (µmol kg^{-1})	Starting DIC (µmol kg^{-1})	TA increase (µmol kg^{-1})	Maximum Ω_A reached	Days of stable TA	Overall TA loss (µmol kg^{-1})	Overall DIC loss (µmol kg^{-1})	Final Ω_A
Salinity effect on $Mg(OH)_2$ dissolution and $CaCO_3$ precipitation kinetics								
Salinity 36 (35.80)	2292.2 ±1.4	2046.40 ±0.88	530.27 ±27.82	9.12 ±0.14	10.33 ±1.53	1030.76 ±32.79	456.71 ±27.91	1.97 ±0.02
Salinity 28 (28.47)	1845.4 ±1.5	1686.35 ±0.55	631.79 ±25.26	9.32 ±0.04	5.33 ±1.15	1087.48 ±23.38	505.92 ±21.66	1.68 ±0.05
Salinity 20 (20.38)	1323.2 ±3.1	1246.08 ±0.53	590.83 ±14.69	8.63 ±0.17	1.67 ±0.58	975.15 ±82.41	535.92 ±62.12	1.52 ±0.01
Grain size effect on $Mg(OH)_2$ dissolution and $CaCO_3$ precipitation kinetics								
Small (<63 µm)	2300.0 ±1.0	2048.18 ±0.50	427.48 ±18.11	8.43 ±0.02	4.67 ±2.08	1009.85 ±18.67	553.35 ±7.79	2.12 ±0.02
Medium (63-180 µm)	2292.2 ±1.4	2046.40 ±0.88	530.27 ±27.82	9.12 ±0.14	10.33 ±1.53	1030.76 ±32.79	456.71 ±27.91	1.97 ±0.02
Large (>180 µm)	2317.3 ±0.6	2056.78 ±1.74	351.25 ±71.78	8.35 ±0.04	2.67 ±0.58	1038.88 ±61.40	638.31 ±28.76	1.93 ±0.02

2.3. Manipulation of dissolved inorganic carbon and magnesium

The seawater dilution by MilliQ to decrease salinity also decreased the concentration of various seawater components, such as Mg and DOC concentrations. To disentangle a potentially general effect of salinity on $Mg(OH)_2$ dissolution and secondary precipitation kinetics from reductions in Mg and DOC concentrations, two additional experiments were designed. In the first, the experiments at a salinity of 20 were replicated, but the Mg concentration was increased to a concentration representative for a salinity of 35, i.e., 52.8 mmol kg^{-1} (Dickson et al., 2007), by magnesium chloride ($MgCl_2$) addition from a 3 M stock solution (molarity verified by inductively coupled plasma mass spectrometer measurements). This experiment was run in triplicate. For the second experiment, a DOC-enriched seawater solution at the salinity of 20 was produced by ultrafiltration (molecular weight cut-off of 2,000 Daltons, Vivaflow200 Hydrosart, Sartorius). A DOC gradient was then created in five bottles by mixing the DOC-enriched salinity 20 seawater with the MilliQ-diluted seawater. The DOC concentrations ranged from approximately 120 µmol kg^{-1} to approximately 325 µmol kg^{-1}.

In both the Mg and DOC experiments, dissolution and secondary $CaCO_3$ precipitation kinetics were mainly monitored by pH_F measurements, although a sample for TA and DIC was also taken before $Mg(OH)_2$ addition and at the end of each treatment. These samples, coupled to the pH_F measurements, allowed the changes in TA and DIC to be estimated over time. The reconstruction occurred in two steps, where the increase in pH following $Mg(OH)_2$ was assumed to be linked to an increase of TA at constant DIC. Then, any decrease in pH was assumed to be due to $CaCO_3$ precipitation, so the estimated TA and DIC loss after $Mg(OH)_2$ dissolution were decreasing in a 2:1 ratio, as observed in the salinity and grain size experiments. Finally, to account for CO_2 ingassing over time, the difference between estimated maximum TA and final measured TA was used as a proxy. Half of the difference, representing $CaCO_3$ precipitation, was used to estimate the theoretical DIC loss. Once compared to the final measured DIC, an ingassing rate was estimated.

2.4. Analytical procedures

The pH electrode was calibrated using three Metrohm buffer solutions (pH 4, 7 and 9), corresponding to a pH measurement on the free scale. TA analyses were conducted using a potentiometric titration with an 848 Titrino Plus, coupled to an 869 Compact Sample Changer from Metrohm. A 0.05M HCl solution with the ionic strength adjusted to 0.72 mol kg^{-1} (representative for a salinity of 35) using NaCl was used as the titrant (Dickson et al., 2007). The DIC concentration was measured using an Automated Infra-Red Inorganic Carbon Analyzer (AIRICA) coupled to a LI-COR Li7000 Infra-Red detector (Gafar and Schulz, 2018). Both TA and DIC measurements were corrected against in-house reference material (previously calibrated against certified reference material), with measurement uncertainties of ±2.20 and ±1.98 µmol kg^{-1} (Moras et al., 2023). Ω_A and carbonate chemistry speciation were calculated from measured TA and DIC, providing temperature and salinity measurements, using CO2SYS (Sharp et al., 2021). To do so, the boric acid dissociation constant

from Uppström (1974), the carbonic acid dissociation constant from Lueker et al. (2000), and the sulfuric acid dissociation constant of Dickson (1990) were selected.

For scanning electron microscopy (SEM), discrete samples of about 10 mL of TA enriched seawater were filtered through 0.2 µm polycarbonate filters (Whatman Cyclopore). These filters were rinsed with 20 mL of MilliQ to remove salts and dried overnight at 60 °C. Once dried, the filters were kept in a desiccator until analysis. The filters were attached to double-sided carbon tabs and placed on aluminium mounts before being coated with gold. SEM analysis was performed using a tabletop Scanning Electron Microscope TM4000 Plus from Hitachi, coupled to an Energy Dispersive X-Ray (EDX) Analyser, allowing to determine the elemental composition of observed particles.

The concentration of the $MgCl_2$ stock solution was measured by inductively coupled plasma mass spectrometer (ICP-MS) measurements using an Agilent 7700 ICP-MS, coupled to a laser ablation unit (NWR213, Electro Scientific Industries, Inc.). Seawater reference materials from the National Research Council of Canada NASS-6 were used to correct the measurements. The DOC concentration of the DOC-enriched stock solution was determined using a Thermo Fisher Flash Elemental Analyzer after acidifying the sample with nitric acid (Carvalho, 2023).

3. Results

3.1. Grain size effects on $Mg(OH)_2$ dissolution kinetics

Three $Mg(OH)_2$ grain sizes were dissolved in seawater at a salinity of ~36 (Figure 1). The starting pH_F was similar for all incubations, with 8.11 ±0.03, 8.09 ±0.01 and 8.07 ±0.03, for the small (<63 µm), medium (63-180 µm) and large (>180 µm) grain sizes, respectively. Upon dissolution, pH_F increased quite rapidly, reaching a maximum after about two hours for the small particle size experiments, and about 6 to 8 hours in the medium and large particle size experiments (Figure 1). In each incubation, a logarithmic trend in pH_F was observed, with the dissolution being much quicker for smaller grain sizes. After two hours, the maximum pH_F recorded for the smaller grain size was 8.76 ±0.04, which continuously decreased to 8.68 ±0.00 between 11 and 12 hours after $Mg(OH)_2$ addition. In contrast, the pH_F for the medium and larger grain size increased to 8.72 ±0.00 and 8.68 ±0.03 after about eight hours and remained stable thereafter, respectively (Figure 1).

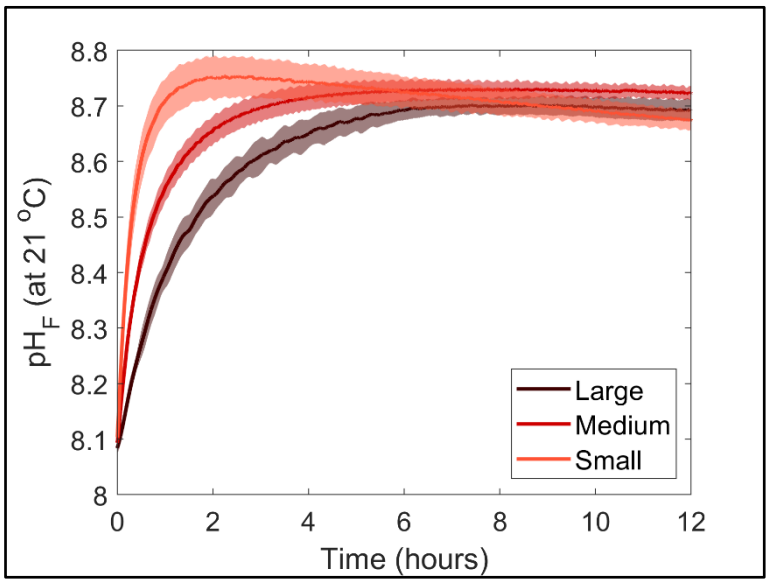

Figure 1: Changes in pH_F at 21 °C following dissolution of three $Mg(OH)_2$ grain sizes in natural seawater over 12 hours. Each grain size was run in triplicate, with the average presented as the solid lines and the standard deviation range as the transparent areas.

3.2. Grain size effect on $CaCO_3$ precipitation kinetics

The pH increase was reflected by increasing TA, measured prior to the $Mg(OH)_2$ addition and 18 hours later, by about 430, 530 and 350 µmol kg^{-1}, in the small, medium and large grain size incubations, respectively (Figure 2). The TA remained stable for 3-7 days, 9-12 days, and 2-3 days before dropping in each grain size treatment (small, medium, large). In all incubations, TA concentrations decreased in a similar fashion, with a strong drop the first two days, before slowly decreasing for another week and stabilising. The overall TA loss for the duration of the experiments was ~1035 µmol kg^{-1} in the medium and large grain size incubations, while the TA dropped by about 1010 µmol kg^{-1} in the small grain size incubations (Table 1).

The changes in Ω_A followed a similar pattern as TA, increasing from ~2.8 on average to ~9.1 in the medium grain size incubation, and to ~8.4 in the small and large grain size experiments. Ω_A dropped at the same time as TA in the respective experiments, stabilising around ~2.0 in all experiments.

Finally, a small drop in DIC was observed after $Mg(OH)_2$ addition in all experiments, of about 80, 30 and 140 µmol kg^{-1} in the small, medium and large grain size incubations, respectively. The DIC remained then relatively stable until the rapid TA drop, where the overall DIC drops for the small, medium and large grain size incubations were calculated at ~550, ~455 and ~640 µmol kg^{-1}, respectively. While TA and Ω_A remained stable after this drop, DIC slightly increased, particularly obvious in the medium and larger grain size incubations.

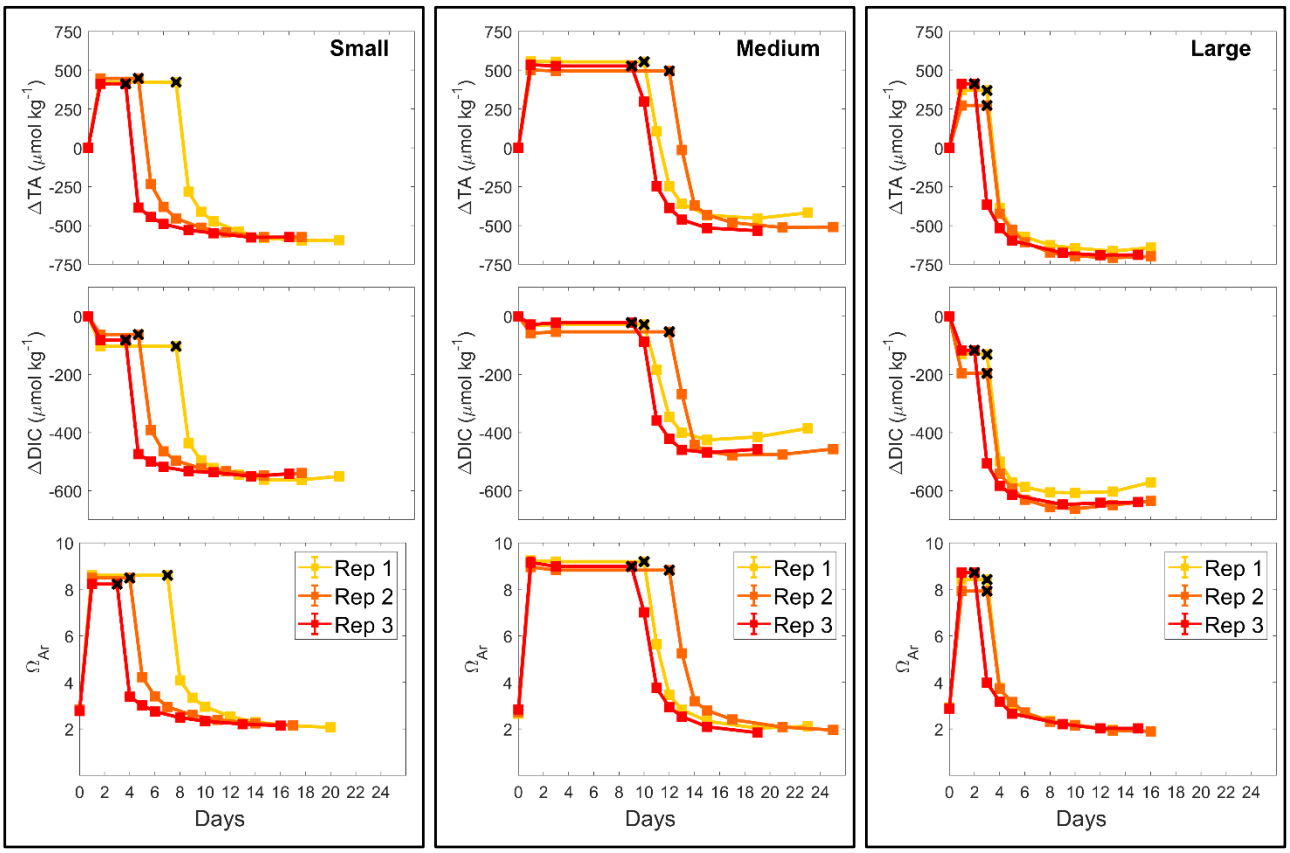

Figure 2: Changes in TA, DIC and Ω_A during dissolution of three $Mg(OH)_2$ grain sizes in natural seawater over up to 25 days. Three replicates were conducted for each grain size and are represented in red, orange and yellow. The last stable TA and DIC conditions estimated by pH_F measurements are represented by a black cross.

3.3. Salinity effect on $Mg(OH)_2$ dissolution kinetics

To test the salinity effect on $Mg(OH)_2$ dissolution and $CaCO_3$ precipitation kinetics, three sets of experiments were conducted in three different salinities, i.e., 20.38, 28.47 and 35.80, and using medium grain size $Mg(OH)_2$. From here on the salinities 20.38, 28.47 and 35.80 will be referred to as salinities 20, 28 and 36, respectively. Similarly to the grain size experiments, the dissolution of $Mg(OH)_2$ occurred rapidly in all three salinities, with the maximum pH_F being recorded after approximately 8 hours (Figure 3). Starting pH_F were slightly different, recorded at 7.99 ±0.05, 8.06 ±0.01 and 8.09 ±0.01 in the salinity 20, 28 and 36 incubations, and increased to a maximum of 9.19, ±0.00, 8.91 ±0.00 and 8.72 ±0.00, respectively. In all incubations, similar logarithmic trends were observed for pH_F (Figure 3).

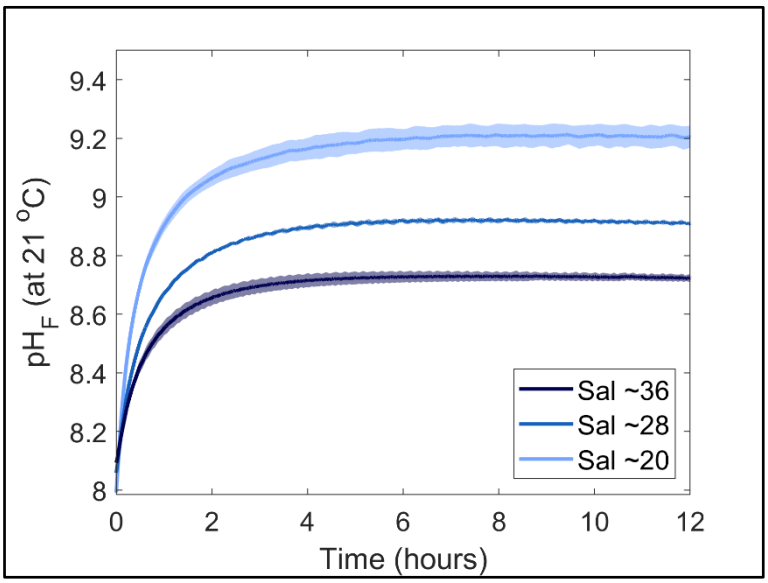

Figure 3: Changes in pH_F at 21 °C following $Mg(OH)_2$ dissolution in three different seawater salinities over 12 hours. Each salinity has been run in triplicate, with the average presented as the solid lines and the standard deviation range as the transparent areas. Please note that different maximum pH levels were reached because of increasing $Mg(OH)_2$ additions with decreasing salinity to reach a similar Ω_A.

3.4. Salinity effect on $CaCO_3$ precipitation kinetics

In all incubations, TA was increased as suggested by the pH_F trends, by ~590, ~630 and ~530 µmol kg^{-1} in the salinity 20, 28 and 36 incubations, respectively (Figure 4). The TA remained stable for different periods of time in each treatment; 1-2 days in the salinity 20 incubations, 4-6 days in the salinity 28 incubations, and 9-12 days in the salinity 36 incubations. Thereafter, TA dropped quickly the first two days in all incubations and stabilised quickly in the salinity 20 experiments. In the salinity 28 incubations, the TA slowly decreased over five days after the first strong drop and stabilised, while in the salinity 36 experiments, the TA decreased slowly after the initial drop over seven days before stabilising. The overall TA losses for salinities 20, 28 and 36 experiments were estimated at ~975, ~1090 and ~1030 µmol kg^{-1}, respectively (Table 1).

Ω_A values followed a similar pattern as TA in all experiments. The starting Ω_A were different, varying between 1.0 for the salinity 20 incubations to 2.0 and 2.8 for the salinity 28 and 36 incubations, respectively. Similarly, following $Mg(OH)_2$ additions, Ω_A quickly increased to reach 8.6, 9.3 and 9.1 with increasing salinity. Together with TA, Ω_A eventually started dropping, and then stabilised at different values, around 1.5 for a salinity of 20, around 1.7 for a salinity of 28 and around 2.0 for a salinity of 36.

Finally, DIC also decreased upon $Mg(OH)_2$ additions. An initial DIC drop was observed directly after $Mg(OH)_2$ additions of about 60 µmol kg^{-1} at the lowest salinity and 30 µmol kg^{-1} at the highest salinity. At a salinity of 28, a much smaller DIC drop was observed in one replicate. After a period of stable DIC conditions, DIC also dropped in a similar fashion

as TA, with an overall DIC loss of about 535, 505 and 455 µmol kg^{-1} from the lower to higher salinity incubations. While no DIC increase was observed towards the end of the experiment in the salinity 36 incubations, strong DIC increases were observed in the salinity 28 incubations and even more prominent ones in the salinity 20 incubations.

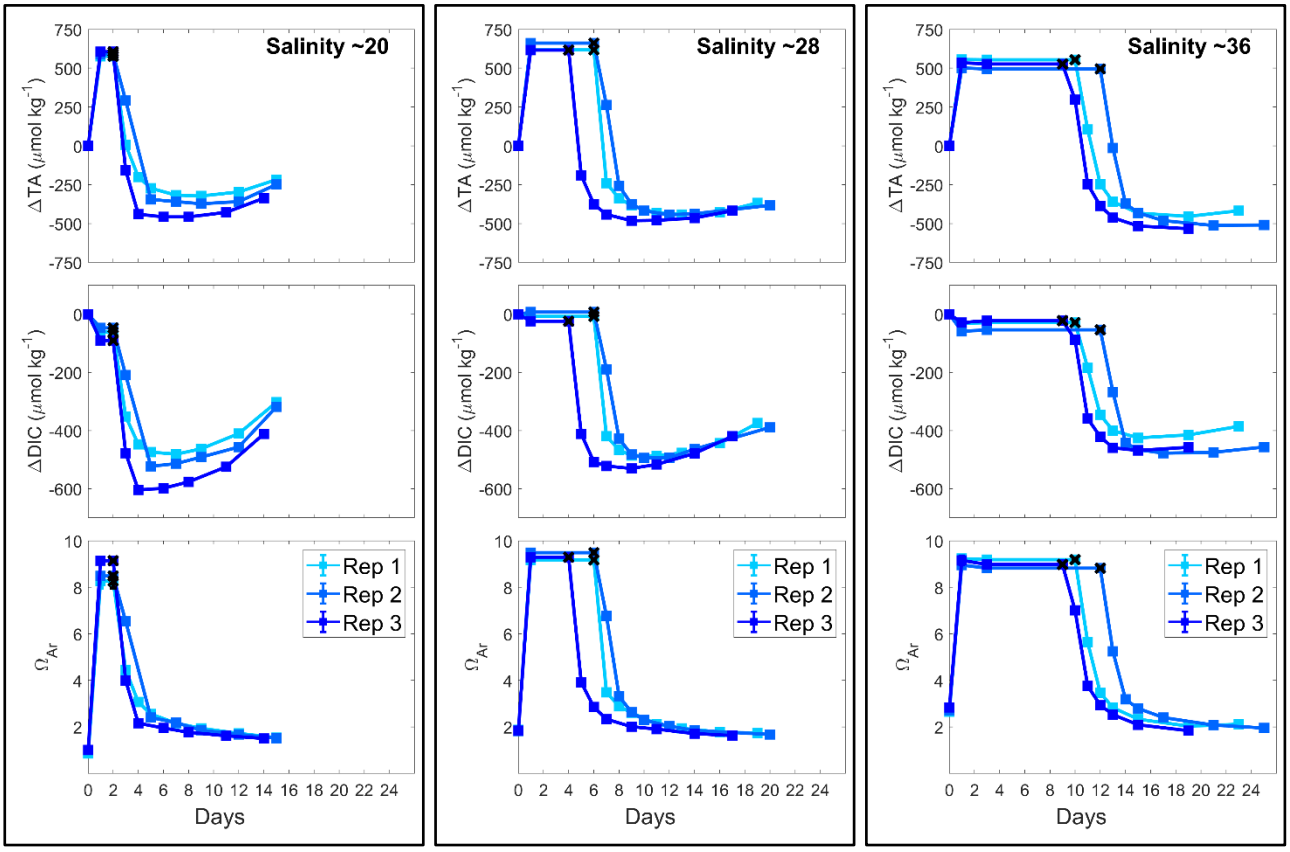

Figure 4: Changes in TA, DIC and Ω_A during $Mg(OH)_2$ dissolution in three different salinities over up to 25 days. Three replicates were conducted for each salinity and are represented in shades of blue. The last stable TA and DIC conditions estimated by pH_F measurements are represented by a black cross.

3.5. Magnesium and DOC effect on $CaCO_3$ precipitation

A similar pattern was observed for the salinity 20 experiments at natural and increased Mg concentrations, i.e., a rapid increase in TA reaching a maximum on day one, followed by a steady decline over the next two weeks (Figure 5). The maximum ΔTA reached was slightly different, with about 600 µmol kg^{-1} of TA increase in the salinity 20, and nearly 800 µmol kg^{-1} in the salinity 20 + $MgCl_2$ incubations. Another interesting difference is the slower TA decrease with $MgCl_2$ compared to the salinity 20. After about 18 days, the lowest ΔTA was reached while it only took about 6 days for the salinity 20 ΔTA to reach the minimum. Similarly, DIC appeared to decrease less rapidly when $MgCl_2$ was present and Ω_A followed a similar trend after the initial strong increase.

Out of the five DOC experiments, four incubations showed a drop in TA (Figure 5). Similar maximum ΔTA were reached in most experiments, with a ΔTA of ~800 µmol kg^{-1}. However, in the incubation with ~120 µmol kg^{-1} DOC, the TA increased only by ~600 µmol kg^{-1}. Following this increase, TA decreased within a day in both 120 and 145 µmol kg^{-1} DOC incubations, and stayed stable until day 3 in incubations with 170 and 220 µmol kg^{-1}. These four incubations also show a similar levelling pattern over time, even though it appears that in the higher DOC incubations, the total loss in TA was lower than for the lower DOC incubations. ΔDIC also follow a similar trend to ΔTA, with an early drop at 120 µmol kg^{-1} of DOC, a drop after one day at 145 µmol kg^{-1} of DOC, and a slow decrease from day 1 and a stronger drop on day 2 at 170 and 220 µmol kg^{-1} of DOC. Ω_A followed a very similar pattern to ΔTA, with final Ω_A being higher in the experiments with higher DOC concentrations. Finally, in the experiment with the highest DOC concentration, i.e., 325 µmol kg^{-1}, no drop in TA, DIC or ΩA was observed (the experiment was run for 42 days).

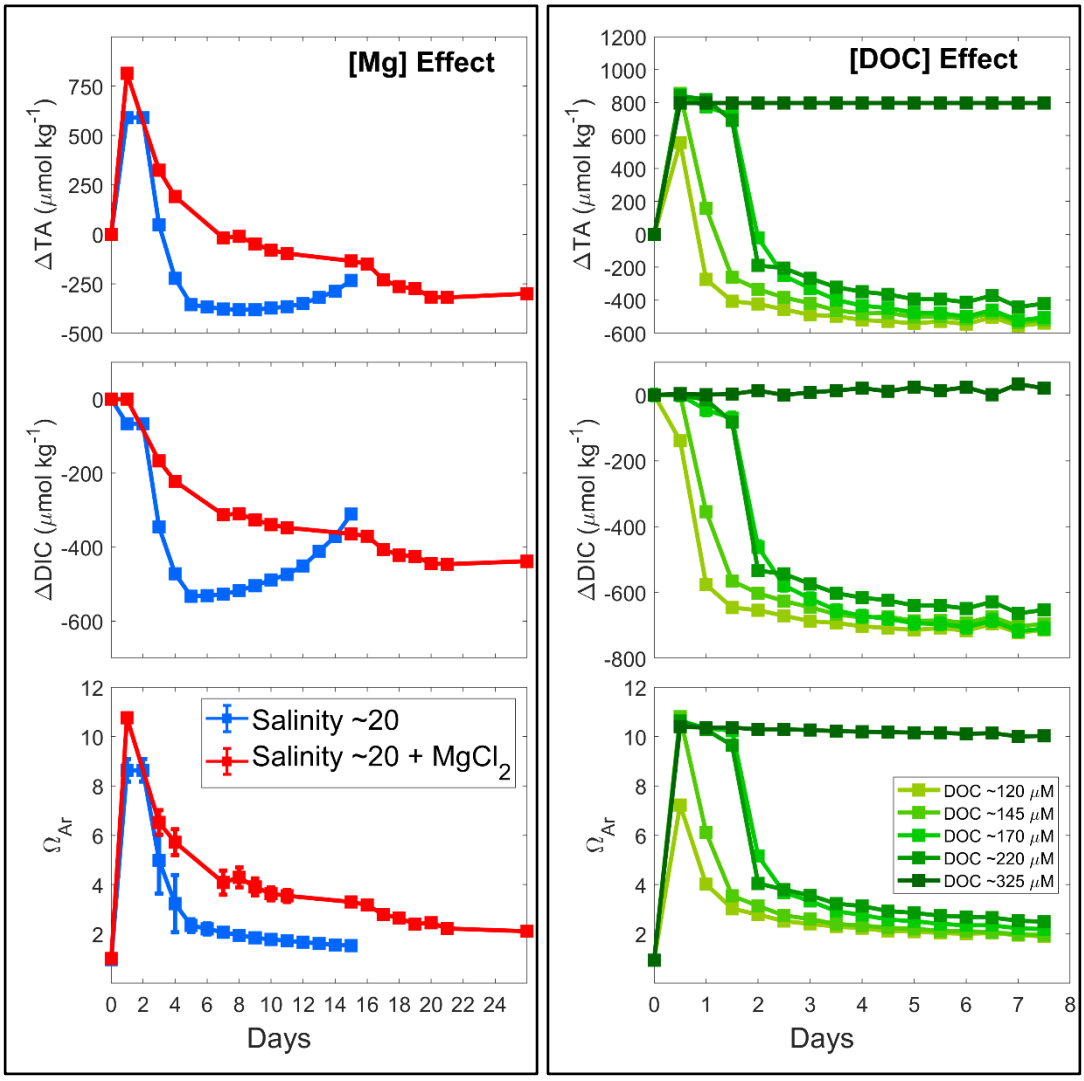

Figure 5: Comparison of the calculated TA, DIC and Ω_A changes at 21 °C following $Mg(OH)_2$ addition in seawater with salinity of 20 (blue), and in seawater with salinity 20 and Mg concentration equal to a salinity 35 (red), and in seawater with varying DOC

concentrations (green). Values reported in the [Mg] Effect graphs represent the average of triplicate experiments run at salinity 20 and salinity 20 + $MgCl_2$, with standard deviations represented by the error bars.

4. Discussion

4.1. Grain size and salinity effects on $Mg(OH)_2$ dissolution

Maximum $Mg(OH)_2$ dissolution directly after its addition was negatively correlated with grain size (Figure 1, Figure 3). The smaller the grain size, the faster the maximum pH_F is reached, indicative of complete dissolution. This can be explained by the fact that smaller particles have a larger surface area per gram of material than larger ones. The increasing dissolution rate with decreasing particle size is particularly noticeable in when TA changes were estimated by using the pH_F data and starting DIC measurements (Figure 6). Assuming a constant DIC over the first 30 minutes of reaction, i.e., no significant $CaCO_3$ precipitation and/or CO_2 ingassing, TA can be reconstructed using CO2SYS. The maximum ΔTA reached with the larger particle size occurred within 8 hours while it only took about 2 hours for the ΔTA to reach a maximum with small particle size. The initial dissolution rate, i.e., within the first 30 minutes, was also significantly different between the various grain sizes. The TA generation of smaller grain size particles was estimated at about 796.5 ±7.1 µmol of TA mg^{-1} min^{-1}. The medium particles dissolved about twice as slow over the first 30 minutes, estimated at 391.6 ±2.6 µmol of TA mg^{-1} min^{-1}, while the larger grain sizes dissolved more than four times slower, with about 168.7 ±6.9 µmol of TA mg^{-1} min^{-1}. Another important difference between the smaller grain size experiments and the two others is the constant decrease in pH_F observed right after reaching the maximum pH_F value (Figure 1). This decrease in pH_F can only be linked to either $CaCO_3$ precipitation, decreasing TA and ultimately pH_F, or CO_2 ingassing, increasing the dissolved CO_2 concentration and ultimately decreasing the pH_F. The constant and linear trend suggest that the latter is responsible for the decrease. If $CaCO_3$ precipitation was responsible for these pH_F changes, the changes would follow a similar pattern to a negative exponential function. This is due to the fact that the more $CaCO_3$ nucleate, the more surface becomes available for further nucleation (Zhong and Mucci, 1989). However, in our case, the changes appear linear. Such a pattern is indicative of CO_2 ingassing at an early stage, i.e., before the ingassing starts plateauing, dictated by the difference between atmospheric and seawater pCO_2. Such ingassing is also occurring in the other experiments, but is likely hidden by the pH_F increase occurring during the longer $Mg(OH)_2$ dissolution with bigger grain size.

For salinity, there was a difference in initial dissolution rates within the range of salinities tested, with dissolution rates for salinities 36, 28 and 20 estimated at 391.6 ±2.6, 359.8 ±0.2 and 301.9 ±0.3 µmol of TA mg^{-1} min^{-1}, respectively. While these differences are not as significant as those in the grain size experiments, the dissolution rate decreased by about 23% between salinity 36 and 20. Overall, TA generation potential of smaller grain size $Mg(OH)_2$ (<63 µm) at a salinity 36 was similar to that of $Ca(OH)_2$ (Moras et al., 2022) which was also sieved through 63 µm. Assuming the same molar TA generation potential, the same maximum Ω_A should have been reached. However, for $Ca(OH)_2$ it was ~7.4, while our small

grain size $Mg(OH)_2$ incubations reached a maximum Ω_A of ~8.4. Such a difference is likely due to the difference in the starting conditions and experimental settings. In the experiments shown here, the starting Ω_A was ~2.8 while it was about ~2.5 in Moras et al. (2022). This is explained by the difference in the starting water composition and salinity, ultimately affecting the final Ω_A despite similar TA increases. Furthermore, higher amounts of $Mg(OH)_2$ were added compared to Moras et al. (2022), leading to a higher Ω_A and a higher theoretical ΔTA, if no early $CaCO_3$ nucleation occurred. However, dissolution kinetics appear to differ between the minerals, with $Ca(OH)_2$ dissolving within 20-30 minutes while it took two hours for $Mg(OH)_2$. These two minerals still dissolve at a relatively quick pace compared to other OAE feedstocks, for instance olivine (Montserrat et al. 2017). Olivine took much longer to dissolve, with a maximum increase in pH recorded of ~0.15 units within 4-9 days. $Ca(OH)_2$ and $Mg(OH)_2$ additions required ~20 mg of materials, while to obtain such olivine results, more than 30 g of olivine were added per kg of filtered seawater, meaning that the TA generation potential is several orders of magnitude lower.

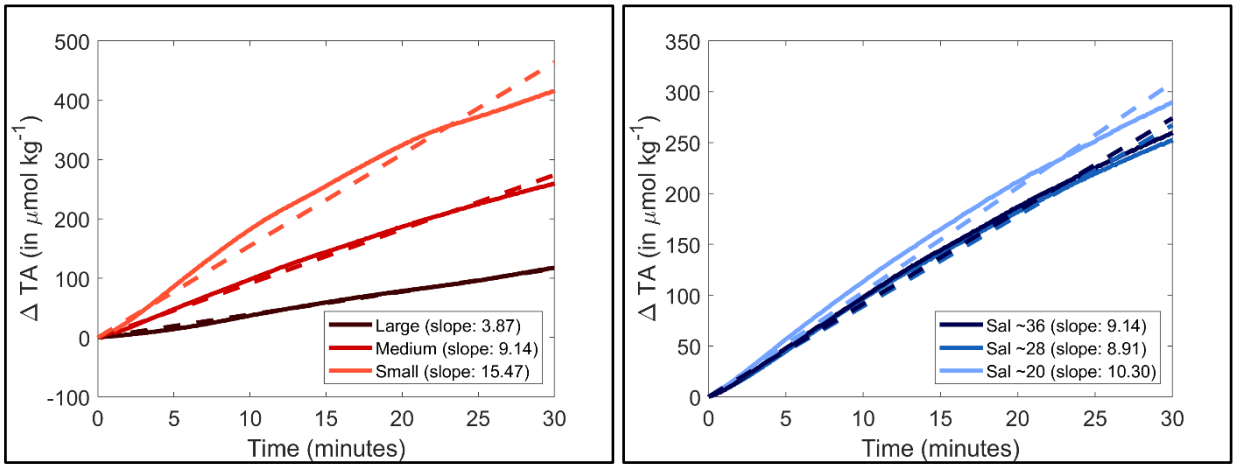

Figure 6: Normalised changes in calculated TA over the first 30 minutes following $Mg(OH)_2$ additions of three different grain sizes in natural seawater (left) and in three different salinities (right). A linear fit was calculated and is represented by the dashed line, and each slope is reported in the legend in between parentheses.

4.2. Grain size and salinity effect on $CaCO_3$ precipitation

In all experiments, $Mg(OH)_2$ additions had been chosen to reach an Ω_A at which secondary $CaCO_3$ precipitation would be expected based on our experience with CaO and $Ca(OH)_2$ (Moras et al., 2022). Based on our suspicion that $CaCO_3$ might precipitate on magnesium-rich particles less easily than onto calcium-rich particles we chose a saturation state of ~9, slightly higher than the level of ~7 observed for CaO and $Ca(OH)_2$ (Moras et al., 2022). Precipitation kinetics were similar for all grain sizes, i.e., after the first precipitation was observed a new steady state was achieved in about two weeks. Precipitation seemingly stopped at Ω_A values close to 2.0 in experiments with seawater at a salinity of 36, similar to observations made by Moras et al. (2022) using CaO and $Ca(OH)_2$. For the smallest grain size, TA was stable for 3-7 days, which is longer than what

has been observed for CaO and $Ca(OH)_2$ at the same size (Moras et al., 2022). This could be related to higher lattice compatibility of $CaCO_3$ for calcium-based minerals when it comes to precipitation onto mineral surfaces (Lioliou et al., 2007). Interestingly, however, the rate at which $CaCO_3$ precipitated was similar for CaO and $Mg(OH)_2$, while $Ca(OH)_2$ took almost twice as long to reach a new steady state (compare Figure 1 with Figure 2 in Moras et al., 2022).

TA remained stable for longer, i.e., 9-12 days with medium grain size. However, similarly to the smaller grain size experiments, the TA was also less stable with the larger grain size, i.e., 2-3 days. As such, there appears to be an optimum grain size for keeping TA stable for longer. To explain this, there must be two opposing processes at work. As discussed earlier, smaller particles have larger surface area per gram of material than larger ones, i.e., smaller particles in our experiments had on average more than 23 times the area of larger particles for the same amount of material, assuming round particles of 63 and 180 µm, respectively. Hence, heterogeneous precipitation will be quicker for smaller particles (Zhong and Mucci, 1989). In contrast, what could favour quicker precipitation for larger particles with smaller surface area remains to be understood. Here, it could be higher pH levels and hence Ω_A that are reached at a particle's surface as of having a larger diffusive boundary layer. Hence, pH and Ω_A levels are likely to be much higher and remain for longer due to the slower dissolution of larger particles at the site of $CaCO_3$ nucleation, which positively affects $CaCO_3$ precipitation rates.

At varying salinities, $CaCO_3$ precipitation became noticeable at different points in time, earlier at low salinity and later at higher salinity. While the first assumption was that at lower salinity, the decrease in [Ca] would prevent early $CaCO_3$ precipitation in lower salinity, it appears that another mechanism is at play. The natural $CaCO_3$ inhibition potential of seawater, due to dissolved Mg and DOC concentration, was affected during MilliQ dilution. It now appears that at lower salinity, the decrease in inhibition allowed for $CaCO_3$ precipitation to occur despite a decrease in [Ca] and starting Ω_A. Under such circumstances, early $CaCO_3$ nucleation on yet to be dissolved $Mg(OH)_2$ particles would occur at a faster rate in lower salinity which could be explained by the early drops in DIC after $Mg(OH)_2$ addition. The absence of such decrease in the salinity 28 experiments is an interesting outcome but could be explained by an early CO_2 ingassing. The increase in DIC through CO_2 ingassing could have compensated for the DIC decrease from early $CaCO_3$ formation.

While EDX analysis did not reveal significant magnesium concentrations in early precipitated aragonite crystals to our surprise, i.e., ~18 hours after $Mg(OH)_2$ addition, some aragonite crystals were observed early on. The presence of Mg could have been expected if $CaCO_3$ precipitated heterogeneously onto $Mg(OH)_2$ particles (Figure 7). The absence of Mg after EDX analysis suggests that while some $Mg(OH)_2$ could have been used as a precipitation nuclei for $CaCO_3$ early on, it completely dissolved within the first 18 hours. Only the freshly precipitation $CaCO_3$ would then remain in suspension, eventually acting as precipitation nuclei for runaway $CaCO_3$ precipitation. Finally, it is interesting to highlight that some traces of early aragonite crystals were present in all experiments, and that the needle-shaped crystals were two to three times smaller in the larger grain size experiments than those sampled at the end of the medium grain size experiments (Figure 7). One

explanation that supports the previously mentioned boundary layer theory is that the larger grain size particles, dissolving at a slower pace, maintained a Mg-rich environment while $CaCO_3$ started nucleating. The presence of this Mg during nucleation could have ultimately prevented $CaCO_3$ to fully form as bigger needle-like crystals. However, these are speculations that are hard to prove or disprove.

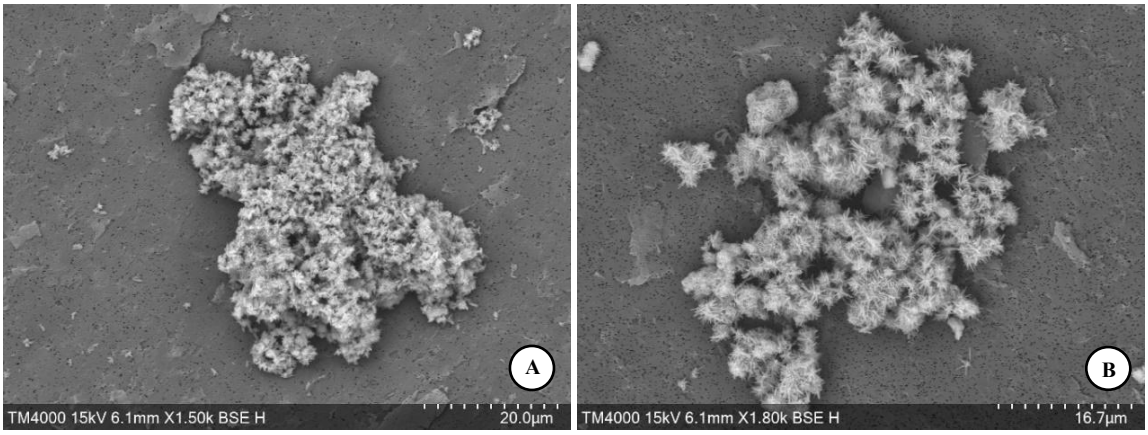

Figure 7: SEM images of aragonite crystals, sampled ~18 hours after larger $Mg(OH)_2$ grain size addition (A) and sampled at the end of the medium grain size incubations (B).

4.3. The role of dilution and potential effects of Mg and DOC concentrations

The role of Mg in inhibiting $CaCO_3$ nucleation is well known (Morse et al., 2007, Pan et al., 2021, Pytkowicz, 1965). Another known $CaCO_3$ nucleation inhibitor is organic matter, particularly dissolved organic matter (Chave and Suess, 1970). While the role of organic matter is not as well understood as Mg, both have been linked to a decrease in $CaCO_3$ nucleation and precipitation rates.

In our experiments involving dilution with MilliQ water, all dissolved components of the seawater were diluted, including Mg and DOC. Such decreases could explain the quicker $CaCO_3$ precipitation in the salinity 20 experiments compared to salinity 36, as lower Mg and DOC concentrations were not inhibiting precipitation as in the higher salinity treatments. To test this, a new salinity 20 batch was prepared in triplicate and Mg was added to raise the total Mg concentration to ~52 mmol kg^{-1}, similar to the Mg concentration in natural seawater at a salinity 35. The Mg increase did affect $CaCO_3$ precipitation kinetics as shown by changes in TA (Figure 5), being slightly slower and apparently reaching a new steady state at higher ΔTA and Ω_A. Furthermore, it is important to highlight that despite $CaCO_3$ precipitation being triggered at a similar time, i.e., within 1 to 2 days, a difference was observed regarding the maximum ΔTA reached. In the salinity 20 + $MgCl_2$ experiments, the maximum ΔTA value was higher than the one in the salinity 20 experiments. This suggests that with a higher dissolved Mg

concentration, less $CaCO_3$ is precipitated early on. Following this early precipitation, an overall slower precipitation rate is observed until reaching a steady state (Figure 5).

However, the slightly reduced $CaCO_3$ precipitation rate due to decreased Mg concentrations alone cannot explain such stark differences in TA stability between the salinity 36 and 20 experiments (Figure 4). It is most likely linked to both the decrease in Mg and DOC concentrations when diluting with MilliQ. The gradient of five salinity 20 replicates with increasing DOC concentrations clearly showed that secondary $CaCO_3$ precipitation could be delayed by modifying the DOC concentrations alone. For instance, secondary precipitation became already measurable after 12 hours at DOC concentrations of 120 µmol kg^{-1}, i.e., salinity 35 diluted to 20, but almost no secondary precipitation at a DOC concentration of 325 µmol kg^{-1}, i.e., about one and a half times higher than in the salinity 35. $CaCO_3$ precipitation was delayed by about two days when doubling DOC concentration, and completely prevented at even higher levels (Figure 5) within the timeframe of the experiment (1 week). Together, these data suggest that seawater DOC and Mg act in synergy when it comes to inhibiting $CaCO_3$ precipitation.

Another interesting finding was the new steady state reached after runaway $CaCO_3$ precipitation. In natural seawater at a salinity of 36, the equilibrated Ω_A was estimated around 2.0, which is about 0.8 units lower than the starting conditions (Figure 4). The decrease in Ω_A after runaway precipitation has important implications for OAE, as when $CaCO_3$ precipitates in a runaway fashion, seawater can become more acidic than it was prior to mineral dissolution and less able to sequester atmospheric CO_2 (Moras et al., 2022). While further work is required to understand these carbonate chemistry mechanisms at lower salinities, we can note that after runaway precipitation in seawater at a salinity of 20, the final Ω_A was higher than the starting one. Such a difference is likely due to the lower starting Ca^{2+} concentration at lower salinity.

5. Conclusions

One main objective of this research was to assess the dissolution of $Mg(OH)_2$ in seawater at varying salinity, and using different mineral grain sizes, and report on the subsequent $CaCO_3$ precipitation kinetics. The dissolution of $Mg(OH)_2$ in natural seawater occurred at a much faster rate when using grain sizes lower than 63 µm, due to the higher surface area in contact with seawater. In contrast, bigger particles (>63 µm) took about four times as long to fully dissolve. In all experiments, $CaCO_3$ precipitation occurred in a runaway fashion, i.e. after a period of seeming stability, TA decreased rapidly before a new steady state was reached at which TA reached concentrations far lower than prior to the $Mg(OH)_2$ addition. Such pattern was also observed for Ca-rich minerals as well, but at lower Ω_A. While further research is required to precisely determine the critical Ω_A for both Ca- and Mg-rich minerals, the longer time for $CaCO_3$ runaway precipitation to be initiated and the overall higher Ω_A may suggest that $Mg(OH)_2$ is a safer alkaline feedstock for OAE. One major finding of this research was that two processes seem to occur during $CaCO_3$ precipitation in relation to grain size, one where the higher surface area of smaller

particles could increase precipitation rates, while the second may maintain a higher pH around larger particles due to a larger diffusive boundary layer compared to smaller particles, which increased precipitation rates. Hence, there appears to be an optimum grain size to minimise secondary $CaCO_3$ precipitation. The second objective of this research was to understand the role of salinity on $Mg(OH)_2$ dissolution and $CaCO_3$ precipitation kinetics. While no obvious changes in dissolution were observed, $CaCO_3$ precipitation differed, with a quicker precipitation observed at lower salinities. The decrease in Mg concentrations was identified as the root cause, although in our experiments it was also linked to a lowered DOC concentration, an artefact of low salinity seawater preparation by dilution with MilliQ. Nevertheless, this highlights the importance of DOC in modifying $CaCO_3$ precipitation kinetics and hence, TA stability.

Data availability

All data were collected by Charly A. Moras and were publicly published on the 05th of June 2024, on the open repository ZENODO under the name "Dataset on the effects of mineral grain size and seawater salinity on $Mg(OH)_2$ dissolution and $CaCO_3$ precipitation kinetics", and can be found at https://doi.org/10.5281/zenodo.11483882.

Author contributions

CAM and KGS designed the initial experiments with inputs from TC and LTB. CAM ran all the experiments and with the help of KGS designed the follow-up experiments with $MgCl_2$ and DOC. The ICP-MS analyses were performed by CAM and RJB, while CAM and KGS performed the SEM analyses. The first draft of the manuscript was written by CAM with inputs from KGS, and all co-authors have helped writing and reviewing the manuscript for submission.

Competing interests

At least one of the (co-)authors is a member of the editorial board of *Biogeosciences*.

Acknowledgments

We would like to sincerely thank Atlas Materials for providing the magnesium hydroxide. We are also thankful to Nick Ward for accommodating the use of the Scanning Electron Microscope, as well as Matheus Carvalho de Carvalho for the dissolved organic carbon analyses.

Financial support

This research is part of the PhD project of Charly A. Moras that is funded by a Cat. 5 – SCU Grad School scholarship from the Southern Cross University, Lismore, Australia. The ICP-MS analyses were made possible by Australian Research Council grants to Renaud Joannes-Boyau and Kai G. Schulz (grant no. LE200100022) and to Renaud Joannes-Boyau (grant no. LE120100201).

References

Carvalho, M. C.: Adapting an elemental analyser to perform high-temperature catalytic oxidation for dissolved organic carbon measurements in water, Rapid Communications in Mass Spectrometry, 37, e9451, 10.1002/rcm.9451, 2023.

Chave, K. E. and Suess, E.: Calcium carbonate saturation in seawater: Effects of dissolved organic matter, Limnology and Oceanography, 15, 633-637, 10.4319/lo.1970.15.4.0633, 1970.

Dickson, A. G.: Standard potential of the reaction: AgCl(s) + 12H2(g) = Ag(s) + HCl(aq), and the standard acidity constant of the ion HSO4− in synthetic sea water from 273.15 to 318.15 K, The Journal of Chemical Thermodynamics, 22, 113-127, 10.1016/0021-9614(90)90074-Z, 1990.

Dickson, A. G., Sabine, C. L., and Christian, J. R.: Guide to best practices for ocean CO_2 measurements, PICES Special Publication 3; IOCCP Report 8, Sidney, British Columbia, North Pacific Marine Science Organization, 191 pp., 10.25607/OBP-1342, 2007.

Eisaman, M. D., Geilert, S., Renforth, P., Bastianini, L., Campbell, J., Dale, A. W., Foteinis, S., Grasse, P., Hawrot, O., Löscher, C. R., Rau, G. H., and Rønning, J.: Assessing the technical aspects of ocean-alkalinity-enhancement approaches, Guide to Best Practices in Ocean Alkalinity Enhancement Research, 2-oae2023, 3, 10.5194/sp-2-oae2023-3-2023, 2023.

Friedlingstein, P., Jones, M. W., O'Sullivan, M., Andrew, R. M., Bakker, D. C. E., Hauck, J., Le Quéré, C., Peters, G. P., Peters, W., Pongratz, J., Sitch, S., Canadell, J. G., Ciais, P., Jackson, R. B., Alin, S. R., Anthoni, P., Bates, N. R., Becker, M., Bellouin, N., Bopp, L., Chau, T. T. T., Chevallier, F., Chini, L. P., Cronin, M., Currie, K. I., Decharme, B., Djeutchouang, L. M., Dou, X., Evans, W., Feely, R. A., Feng, L., Gasser, T., Gilfillan, D., Gkritzalis, T., Grassi, G., Gregor, L., Gruber, N., Gürses, Ö., Harris, I., Houghton, R. A., Hurtt, G. C., Iida, Y., Ilyina, T., Luijkx, I. T., Jain, A., Jones, S. D., Kato, E., Kennedy, D., Klein Goldewijk, K., Knauer, J., Korsbakken, J. I., Körtzinger, A., Landschützer, P., Lauvset, S. K., Lefèvre, N., Lienert, S., Liu, J., Marland, G., McGuire, P. C., Melton, J. R., Munro, D. R., Nabel, J. E. M. S., Nakaoka, S. I., Niwa, Y., Ono, T., Pierrot, D., Poulter, B., Rehder, G., Resplandy, L., Robertson, E., Rödenbeck, C., Rosan, T. M., Schwinger, J., Schwingshackl, C., Séférian, R., Sutton, A. J., Sweeney, C., Tanhua, T., Tans, P. P., Tian, H., Tilbrook, B., Tubiello, F., van der Werf, G. R., Vuichard, N., Wada, C., Wanninkhof, R., Watson, A. J., Willis, D., Wiltshire, A. J., Yuan, W., Yue, C., Yue, X., Zaehle, S., and Zeng, J.: Global carbon budget 2021, Earth System Science Data, 14, 1917-2005, 10.5194/essd-14-1917-2022, 2022.

Fuhr, M., Geilert, S., Schmidt, M., Liebetrau, V., Vogt, C., Ledwig, B., and Wallmann, K.: Kinetics of Olivine Weathering in Seawater: An Experimental Study, Frontiers in Climate, 4, 10.3389/fclim.2022.831587, 2022.

Gafar, N. A. and Schulz, K. G.: A three-dimensional niche comparison of Emiliania huxleyi and Gephyrocapsa oceanica: reconciling observations with projections, Biogeosciences, 15, 3541-3560, 10.5194/bg-15-3541-2018, 2018.

GESAMP: High level review of a wide range of proposed marine geoengineering techniques. (Boyd, P.W. and Vivian, C.M.G., eds.). (IMO/FAO/UNESCO-IOC/UNIDO/WMO/IAEA/UN/UN Environment/UNDP/ISA Joint Group of Experts on the Scientific Aspects of Marine Environmental Protection). Rep. Stud. GESAMP No. 98, 144 p.1020-4873, 2019.

Gore, S., Renforth, P., and Perkins, R.: The potential environmental response to increasing ocean alkalinity for negative emissions, Mitigation and Adaptation Strategies for Global Change, 24, 1191-1211, 10.1007/s11027-018-9830-z, 2019.

Hartmann, J., Suitner, N., Lim, C., Schneider, J., Marín-Samper, L., Arístegui, J., Renforth, P., Taucher, J., and Riebesell, U.: Stability of alkalinity in ocean alkalinity enhancement (OAE) approaches – consequences for durability of CO_2 storage, Biogeosciences, 20, 781-802, 10.5194/bg-20-781-2023, 2023.

Hartmann, J., West, A. J., Renforth, P., Köhler, P., De La Rocha, C. L., Wolf-Gladrow, D. A., Dürr, H. H., and Scheffran, J.: Enhanced chemical weathering as a geoengineering strategy to reduce atmospheric carbon dioxide, supply nutrients, and mitigate ocean acidification, Reviews of Geophysics, 51, 113-149, 10.1002/rog.20004, 2013.

Hoegh-Guldberg, O., Jacob, D., Taylor, M., Guillén Bolaños, T., Bindi, M., Brown, S., Camilloni, I. A., Diedhiou, A., Djalante, R., Ebi, K., Engelbrecht, F., Guiot, J., Hijioka, Y., Mehrotra, S., Hope, C. W., Payne, A. J., Pörtner, H.-O., Seneviratne, S. I., Thomas, A., Warren, R., and Zhou, G.: The human imperative of stabilizing global climate change at 1.5 °C, Science, 365, eaaw6974, 10.1126/science.aaw6974, 2019.

IPCC: Summary for Policymakers. In: Climate Change 2021: The Physical Science Basis. Contribution of Working Group I to the Sixth Assessment Report of the Intergovernmental Panel on Climate Change [Masson-Delmotte, V., P. Zhai, A. Pirani, S.L. Connors, C. Péan, S. Berger, N. Caud, Y. Chen, L. Goldfarb, M.I. Gomis, M. Huang, K. Leitzell, E. Lonnoy, J.B.R. Matthews, T.K. Maycock, T. Waterfield, O. Yelekçi, R. Yu, and B. Zhou (eds.)], Cambridge University Press, Cambridge, United Kingdom and New York, NY, USA, pp. 3-32, 10.1017/9781009157896.001, 2021.

Kheshgi, H. S.: Sequestering atmospheric carbon dioxide by increasing ocean alkalinity, Energy, 20, 915-922, 10.1016/0360-5442(95)00035-F, 1995.

Lewis, E. L. and Perkin, R. G.: The practical salinity scale 1978: conversion of existing data, Deep Sea Research Part A. Oceanographic Research Papers, 28, 307-328, 10.1016/0198-0149(81)90002-9, 1981.

Lioliou, M. G., Paraskeva, C. A., Koutsoukos, P. G., and Payatakes, A. C.: Heterogeneous nucleation and growth of calcium carbonate on calcite and quartz, Journal of Colloid and Interface Science, 308, 421-428, 10.1016/j.jcis.2006.12.045, 2007.

Lueker, T. J., Dickson, A. G., and Keeling, C. D.: Ocean pCO_2 calculated from dissolved inorganic carbon, alkalinity, and equations for K1 and K2: Validation based on laboratory measurements of CO_2 in gas and seawater at equilibrium, Marine Chemistry, 70, 105-119, 10.1016/S0304-4203(00)00022-0, 2000.

Lüthi, D., Le Floch, M., Bereiter, B., Blunier, T., Barnola, J.-M., Siegenthaler, U., Raynaud, D., Jouzel, J., Fischer, H., Kawamura, K., and Stocker, T. F.: High-resolution carbon dioxide concentration record 650,000–800,000 years before present, Nature, 453, 379-382, 10.1038/nature06949, 2008.

Marion, G. M., Millero, F. J., and Feistel, R.: Precipitation of solid phase calcium carbonates and their effect on application of seawater SA - T - P models, Ocean Science, 5, 285-291, 10.5194/os-5-285-2009, 2009.

Millero, F., Huang, F., Zhu, X., Liu, X., and Zhang, J.-Z.: Adsorption and desorption of phosphate on calcite and aragonite in seawater, Aquatic Geochemistry, 7, 33-56, 10.1023/A:1011344117092, 2001.

Monnin, E., Indermühle, A., Dällenbach, A., Flückiger, J., Stauffer, B., Stocker, T. F., Raynaud, D., and Barnola, J. M.: Atmospheric CO_2 concentrations over the last glacial termination, Science, 291, 112-114, 10.1126/science.291.5501.112, 2001.

Montserrat, F., Renforth, P., Hartmann, J., Leermakers, M., Knops, P., and Meysman, F. J. R.: Olivine dissolution in seawater: Implications for CO_2 sequestration through enhanced weathering in coastal environments, Environmental Science & Technology, 51, 3960-3972, 10.1021/acs.est.6b05942, 2017.

Moras, C. A., Bach, L. T., Cyronak, T., Joannes-Boyau, R., and Schulz, K. G.: Ocean alkalinity enhancement – avoiding runaway $CaCO_3$ precipitation during quick and hydrated lime dissolution, Biogeosciences, 19, 3537-3557, 10.5194/bg-19-3537-2022, 2022.

Moras, C. A., Bach, L. T., Cyronak, T., Joannes-Boyau, R., and Schulz, K. G.: Preparation and quality control of in-house reference materials for marine dissolved inorganic carbon and total alkalinity measurements, Limnology and Oceanography: Methods, 10.1002/lom3.10570, 2023.

Morse, J. W., Arvidson, R. S., and Lüttge, A.: Calcium carbonate formation and dissolution, Chemical Reviews, 107, 342-381, 10.1021/cr050358j, 2007.

Pan, Y., Li, Y., Ma, Q., He, H., Wang, S., Sun, Z., Cai, W.-J., Dong, B., Di, Y., Fu, W., and Chen, C.-T. A.: The role of Mg2+ in inhibiting $CaCO_3$ precipitation from seawater, Marine Chemistry, 237, 104036, 10.1016/j.marchem.2021.104036, 2021.

Pytkowicz, R. M.: Rates of inorganic calcium carbonate nucleation, The Journal of Geology, 73, 196-199, 10.1086/627056, 1965.

Sharp, J., Pierrot, D., Humphreys, M., Epitalon, J., Orr, J., Lewis, E., and Wallace, D.: CO2SYSv3 for MATLAB, Zenodo [code], 10, 10.5281/zenodo.3950562, 2021.

Siegenthaler, U., Stocker, T. F., Monnin, E., Lüthi, D., Schwander, J., Stauffer, B., Raynaud, D., Barnola, J. M., Fischer, H., Masson-Delmotte, V., and Jouzel, J.: Stable carbon cycle-climate relationship during the Late Pleistocene, Science, 310, 1313-1317, 10.1126/science.1120130, 2005.

Uppström, L. R.: The boron/chlorinity ratio of deep-sea water from the Pacific Ocean, Deep Sea Research and Oceanographic Abstracts, 21, 161-162, 10.1016/0011-7471(74)90074-6, 1974.Zeebe, R. E. and Wolf-Gladrow, D.: CO_2 in seawater: equilibrium, kinetics, isotopes, 65, Gulf Professional Publishing, 360 pp.2001.

Zhong, S. and Mucci, A.: Calcite and aragonite precipitation from seawater solutions of various salinities: Precipitation rates and overgrowth compositions, Chemical Geology, 78, 283-299, 10.1016/0009-2541(89)90064-8, 1989.